Indian Journal of Chemical Technology
Vol. 29, July 2022, pp. 354-366

Structured composites between $MnTa_2O_6$ and porphyrins: Influence of the number of carboxylic groups grafted on porphyrins on the capacity to inhibit corrosion of steel

Mihaela Birdeanu[1], Camelia Epuran[2], Ion Fratilescu[2] & Eugenia Fagadar-Cosma*[,2]

[1]National Institute for Research and Development in Electrochemistry and Condensed Matter, Dr. Aurel Paunescu Podeanu Street 144, 300569 Timisoara, Romania

[2]Institute of Chemistry "Coriolan Dragulescu", Mihai Viteazu Ave. 24, 300223 Timisoara, Romania

E-mail: efagadar@yahoo.com

Received 8 January 2022; accepted 24 March 2022

New sandwich type materials based on $MnTa_2O_6$ and porphyrins mono- and tetra-substituted with –COOH groups, namely: (tetrakis-(4-carboxy-phenyl)-porphyrin and 5-(4-carboxy-phenyl)-10,15,20-tris-phenyl-porphyrin) have been synthesized and studied to assess the importance of its corrosion inhibition ability on with regard to its of steel the number of –COOH anchors. Morphological investigations on thin films have been carried out by atomic force microscopy. The inhibition of corrosion has been evaluated by open circuit potential measurements and potentiodynamic polarization technique with Tafel representation, after drop-casting deposition onto carbon steel in 0.1M HCl media. The inhibition efficiency of the novel sandwich-type materials based on pseudo-binary oxide $MnTa_2O_6$ and tetrakis-(4-carboxy-phenyl)-porphyrin or 5-(4-carboxy-phenyl)-10,15,20-tris-phenyl-porphyrin is in the range 76-86% for tetra substituted porphyrin and 84-95% for the mono-COOH substituted porphyrin.

Keywords: Corrosion inhibition, New materials, Porphyrins, Pseudo-binary, Tafel curves, XRD

The corrosion of materials has continued to interest scientists in their endeavor to search for better coating materials and efficient technological methods for obtaining uniformly coated layers on the metallic substrates of various geometric configurations in order to avoid or at least decrease the destruction of metals[1-8].

Coating of steel with corrosion inhibitors, especially based on pseudo-binary oxides and/or porphyrins, leads to significant reduction of the corrosion in aggressive acid media thus increasing the lifetime of the protected installations[9-15].

A single layer of $ZnTa_2O_6$ pseudo-binary oxide deposited by PLD on steel provided an inhibition efficiency of 38.87% in 0.1M NaCl solution[16]. The composition containing a larger amount of zinc, $Zn_3Ta_2O_8$, deposited by PLD as single layer on carbon steel can produce an inhibition efficiency of 24.52 % in 0.1M Na_2SO_4 solutions[17].

Sandwich layers containing two pseudo-binary oxides were tested for assessing their performance with respect to the corrosion protection of steel. Thus $ZnV_2O_6/ZnTa_2O_6$ deposited by PLD showed a significantly increased corrosion inhibition efficiency of 88.46 % in aggressive 0.1M HCl acid medium[18]. Overlapping layers of other metals pseudo-binary oxides, $MgTa_2O_8/MgNb_2O_8$ presented similar corrosion inhibition efficiency, of 87.03%, when deposited onto steel, in 0.05M H_2SO_4 medium[19]. The method of obtaining of the pseudo-binary oxides has a great influence on the corrosion inhibiting properties. For instance, $ZnTa_2O_6$ obtained by hydrothermal method was the most efficient when associated with ZnV_2O_6, in double layers, giving a result of 88.29 % inhibition efficiency in 0.1M NaCl solution[20]. In the last decade, tantalum and manganese contained in different pseudo-binary oxides were widely taken into account for corrosion inhibition approaches due to their excellent results obtained in several aggressive environments[21-36]. On the other hand, porphyrin-base compounds, solely or involved in composite layers with diverse mixed metal oxides, may form physical or even chemical bonds with metal substrate to be protected, showing an already recognized potential as corrosion inhibitors[37,38].

Porphyrins of different structures[17] and their Zn-metalloporphyrins[16,39], have been investigated solely or in several bilayer structured compositions with a conducting polymer (poly-aniline) or with pseudo-binary oxides ($Zn_3Ta_2O_8$, $Zn_3V_2O_8$ and $Zn_3Nb_2O_8$)

providing inhibition efficiencies higher than 80% for carbon steel samples. Mixed substituted A_3B porphyrins possessing one pyridyl substituent and other three inductive electron donor groups, such as: 5-(4-pyridyl)-10,15,20-tris(phenoxy-phenyl)-porphyrin(PyTFen) and 5-(4-pyridyl)-10,15,20-tris(3,4-dimethoxy-phenyl) porphyrin have been tested and gave the best protecting results.

The present study is focused on enhancing corrosion inhibition of modified steel electrodes with thin layers of $MnTa_2O_6$ pseudo-binary oxide and with one of the two different porphyrins, namely: tetrakis-(4-carboxy-phenyl)-porphyrin or 5-(4-carboxy-phenyl)-10,15,20-tris-phenyl-porphyrin, in order to highlight the contribution of the number of –COOH grafted groups. The layers were deposited using the drop-casting technique, in single or sandwich type structures on carbon steel disks. The corrosion tests were performed in 0.1 M HCl media.

Experimental Section

General method for obtaining $MnTa_2O_6$ nanomaterials

The pseudo-binary oxides $MnTa_2O_6$ nanomaterials were obtained by solid-state method using the molar ratios 1:1 between Mn-precursor and Ta-precursor. The starting materials used during the synthesis were: tantalum (V) oxide - Ta_2O_5 (99.99%, Merck), and manganese oxide -MnO (99.99%, Merck), respectively tantalum (V) oxide - Ta_2O_5 (99.99%, Merck), and manganese nitrate tetrahydrate $Mn(NO_3)_2{\times}4H_2O$ (99.99%, Sigma-Aldrich).The obtained materials were in the form of powders and these were subsequently heated at 1100°C for a soaking time of 6 h. The samples were heated and cooled in a furnace at a rate of 5°C min^{-1}.

The X-ray diffraction patterns for: a) $MnTa_2O_6$ (from manganese oxide), b) $MnTa_2O_6$ (from manganese nitrate tetrahydrate) are presented in Fig 1**,** from which it could be observed that besides the main peaks associated with the $MnTa_2O_6$ pure nanomaterials, some associated peaks appeared indexed with JCPDS, card No. 01-072-0485, belonging to the Pbcn space group.

The intensity of the peaks, relative to the background signal, demonstrates the high purity and good quality of the samples.

The highest intensity peak is located at $2\theta = 29.8°$ for $MnTa_2O_6$ which belong to the 311 plane.

The lattice constants for $MnTa_2O_6$ were calculated from XRD analysis data, using Full Prof Suite computer package: a = 14.46 Å, b = 5.78 Å, c = 5.11 Å, $\alpha = \beta = \gamma = 90°$and the elementary cell volume ($V / 10^6 / pm^3$) is 421.54.

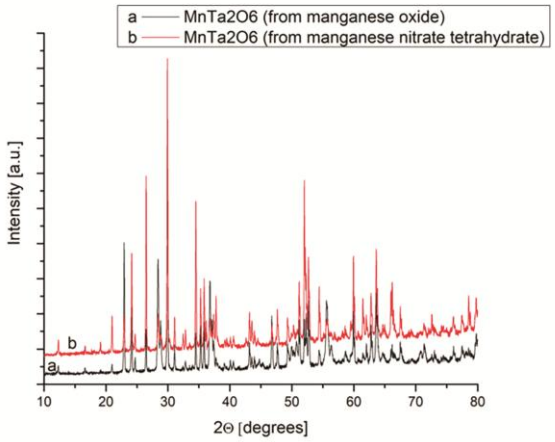

Fig. 1 — XRD patterns of: a) $MnTa_2O_6$ (from manganese oxide), b) $MnTa_2O_6$ (from manganese nitrate tetrahydrate).

The micrographs aspects of the resulting powders were examined by SEM, as shown in Fig 2. for: a) $MnTa_2O_6$ (from manganese oxide), b) $MnTa_2O_6$ (from manganese nitrate tetrahydrate) nanomaterials.

The morphology revealed the formation of soft spherical or ovoid type agglomerates with uniform lace covering aspect (both mesopores and macropores were present).

Method for obtaining carboxyl-substituted A_4 and A_3B porphyrins

The A_3B asymmetrical porphyrin, 5-(4-carboxy-phenyl)-10,15,20-tris-phenyl-porphyrin was obtained by Adler-Longo multicomponent reaction method and fully characterized, as described in previous published report[40].

The tetrakis-(4-carboxy-phenyl)-porphyrin was synthesized by Lindsey method[41] using *p*-methoxy-carbonyl-benzaldehyde, $BF_3.OEt_2$ and chloranil. Final step was the hydrolysis in aqueous HCl solution (35%).

The aspect of porphyrin aggregates is different, as revealed in STEM images from Figs 3(a) and 3(b). The tetra carboxylic substituted porphyrin is organized in perfect spheres with diameters varying from 70-300 nm, while the mono-COOH substituted porphyrin forms ovoid type architectures of more uniform larger dimensions (around 2 µm in the higher diameter).

Design of the structured coverings Method of deposition Equipment

All materials, $MnTa_2O_6$ pseudo-binary oxide, tetrakis-(4-carboxy-phenyl)-porphyrin and 5-

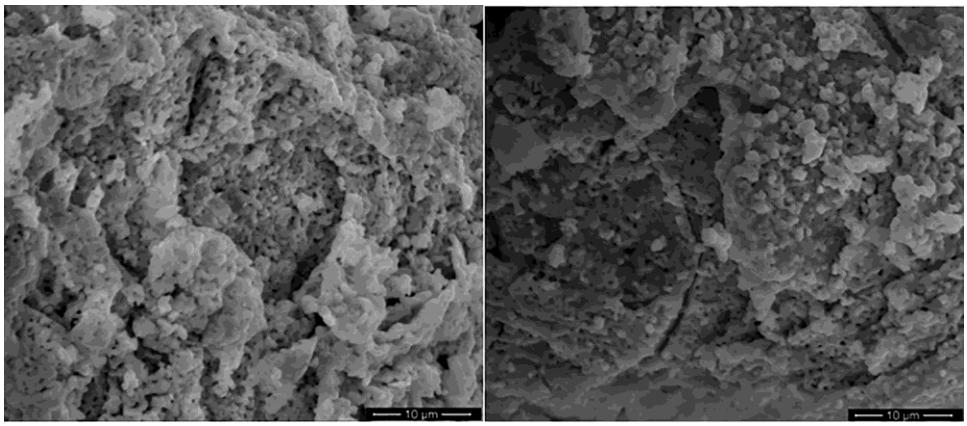

Fig. 2 — SEM micrographs of: a) $MnTa_2O_6$ (from manganese oxide), b) $MnTa_2O_6$ (from manganese nitrate tetrahydrate).

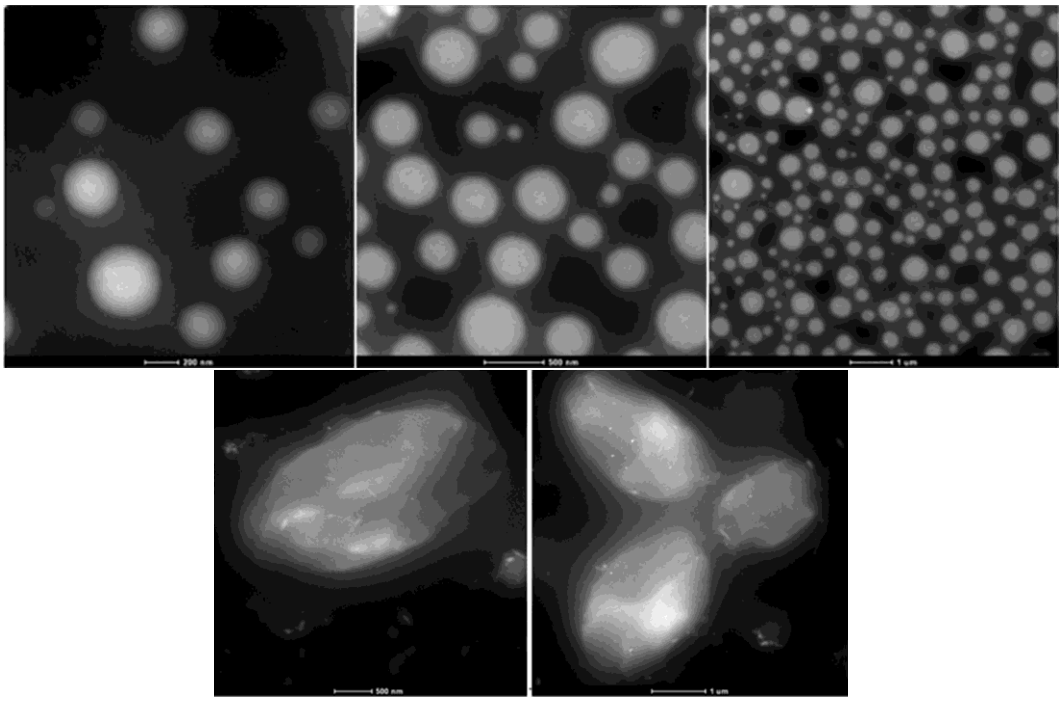

Fig. 3 — (a) STEM images (80 kV) of tetrakis-(4-carboxy-phenyl)-porphyrin from THF and (b)STEM images (80 kV) of 5-(4-carboxy-phenyl)-10,15,20-tris-phenyl-porphyrin from THF.

(4-carboxy-phenyl)-10,15,20-tris-phenyl-porphyrin, were used to obtain single or sandwich type structures by drop casting technique on carbon steel AISI 1144 (OL) disks electrodes (10 mm diameter and 2 mm thick).

The deposition order and the combinations of the layers in the sandwich structures are presented in Table 1.

The morphologies of the obtained single and sandwich structures obtained by drop-casting were investigated by atomic force microscopy on AFM (Model Nanosurf Easy Scan 2 Advanced Research) using the noncontact mode cantilever (scan size of 1.1 μm × 1.1 μm). Electrochemical measurements were performed using a Voltalab potentiostat (Model PGZ 402). Disks of carbon steel AISI 1144 (OL) containing (wt%): 97.54 - 98.01% Fe; 0.4 - 0.44% C; 1.35 - 1.65% Mn; 0.04% max P; 0.24 - 0.33% S were employed as working electrodes.

Before each thin film deposition, the carbon steel disk surfaces were polished to a mirror-like surface, finished by using emery paper, rinsing further with double distilled water and finally degreasing with ethanol.

To investigate the corrosion inhibition capacities of the realized thin films, electrochemical measurements

Table 1 —Drop casting thin film depositions

Sample	Target material and deposition order	Deposition Mode
a	$MnTa_2O_6$ (from manganese oxide)	Single structure
b	$MnTa_2O_6$ (from manganese nitrate tetrahydrate)	Single structure
c	tetrakis-(4-carboxy-phenyl)-porphyrin	Single structure
d	5-(4-Carboxy-phenyl)-10,15,20-tris-phenyl-porphyrin	Single structure
e	$MnTa_2O_6$ (from manganese oxide) / tetrakis-(4-carboxy-phenyl)-porphyrin	Sandwich structure
f	$MnTa_2O_6$ (from manganese oxide) / 5-(4-carboxy-phenyl)-10,15,20-tris-phenyl-porphyrin	Sandwich structure
g	$MnTa_2O_6$ (from manganese nitrate tetrahydrate) / tetrakis-(4-carboxy-phenyl)-porphyrin	Sandwich structure
h	$MnTa_2O_6$ (from manganese nitrate tetrahydrate) / 5-(4-carboxy-phenyl)-10,15,20-tris-phenyl-porphyrin	Sandwich structure
k	Tetrakis-(4-carboxy-phenyl)-porphyrin / $MnTa_2O_6$ (from manganese oxide)	Sandwich structure
l	Tetrakis-(4-carboxy-phenyl)-porphyrin / $MnTa_2O_6$ (from manganese nitrate tetrahydrate)	Sandwich structure
m	5-(4-Carboxy-phenyl)-10,15,20-tris-phenyl-porphyrin / $MnTa_2O_6$ (from manganese oxide)	Sandwich structure
n	5-(4-Carboxy-phenyl)-10,15,20-tris-phenyl-porphyrin / $MnTa_2O_6$ (from manganese nitrate tetrahydrate)	Sandwich structure

were performed. The measurements were performed using a Voltalab Model PGZ 402 potentiostat coupled with a three electrode electrochemical cell, comprised of: bare (OL) or drop casting modified alloy steel tubes disk as working electrode, a platinum wire as counter electrode and a saturated calomel electrode as reference electrode (SCE). The working electrodes were mounted in a Teflon body to ensure a controlled active surface. The potentiodynamic polarization measurements were recorded at 23°C, by sweeping the potential in the -1.3 V ÷ -0.6 V range at a scan rate of 1 mV/s. The open circuit potential (OCP) of the modified electrodes was monitored for 30 min before polarization. The electrolyte solution used for the corrosion tests was 0.1M HCl. The degree of inhibition efficiency (IE) was calculated based on the equation published in literature[42].

Results and Discussion

Morphological characterization

Figure 4 shows AFM images recorded for various single and sandwich structures based on combinations of pseudo-binary oxides and porphyrins before and after corrosion tests in 0.1M HCl media. The surface features are significantly changed after the corrosion test in unprotected carbon steel consisting in the formation of large channels.

Regarding the covered steel electrodes, the main changes are also consisting in the generation of large channels or pores, but there are also morphologic transformations, such as in cases of electrodes (e, f, g, h, k, m and n from Fig 4), that consist also in a rearrangement of the aggregates, from triangular or shell type architectures to smoother films that are continuously covering the surface without any break. The surface roughness - the average roughness (S_a) and the mean square root roughness (S_q) – were calculated from AFM data, using the Nanosurf Easy Scan 2 software, for each covered electrode[43].

The nanorugosity and the particle dimensions were calculated for each of the deposited surface (Table 2). It can be observed that the sandwich structures have increased values of the nanorugosity. The highest value of nanorugosity is in the case thin films deposed with 5-(4-carboxy-phenyl)-10,15,20-tris-phenyl-porphyrin / $MnTa_2O_6$ (obtained from manganese nitrate tetrahydrate) and has a value of 49.42 nm. The thickness of the layers (S_y) was also calculated for each deposition.

Polarisation curves

Fig. 5 shows the OCP versus time for bare and modified carbon steel disk electrodes in 0.1 M HCl electrolyte solution for 30 min. The drop-casting deposited layers determined the shifting of the OCP of the electrodes toward more positive values, compared with the non-protected OL electrode.

The OCP measurements (Fig. 5) showed that all the deposited layers, no matter of their composition or complexity, stabilized the electrodes around 800 s.

The Tafel plots (potential vs. log current density) of the OL disk electrodes modified by drop casting deposition, recorded in 0.1M HCl solution, are displayed in Fig 6. The kinetic parameters obtained from Tafel plots are presented in Table 3.

The thin films obtained by depositing the pseudo-binary oxides on top of the porphyrin layer exhibited a significantly lower corrosion current density (hence a better corrosion inhibition efficiency) than the rest of the protected disk electrodes. This can be explained by an adherent coverage provided by the porphyrins in contact with steel that is further improved in

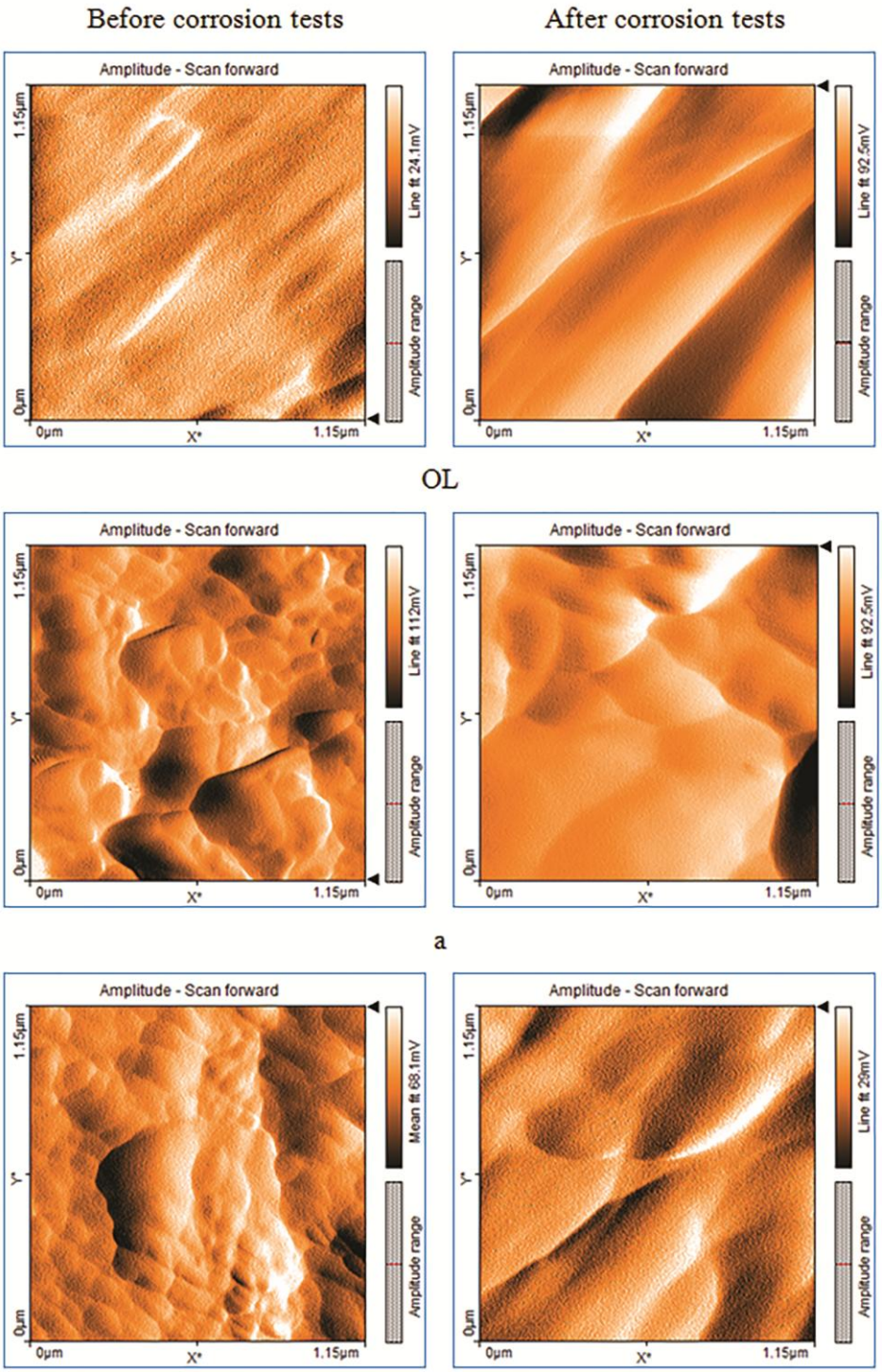

Fig. 4 — 2D AFM images for the depositions with the following structures before and after corrosion tests: OL (bare electrode), a) $MnTa_2O_6$ (from manganese oxide); b) $MnTa_2O_6$ (from manganese nitrate tetrahydrate); c) tetrakis-(4-carboxy-phenyl)-porphyrin; d) 5-(4-carboxy-phenyl)-10,15,20-tris-phenyl-porphyrin; e) $MnTa_2O_6$ (from manganese oxide) / tetrakis-(4-carboxy-phenyl)-porphyrin; f) $MnTa_2O_6$ (from manganese oxide) / 5-(4-carboxy-phenyl)-10,15,20-tris-phenyl-porphyrin; g) $MnTa_2O_6$ (from manganese nitrate tetrahydrate) / tetrakis-(4-carboxy-phenyl)-porphyrin; h) $MnTa_2O_6$ (from manganese nitrate tetrahydrate) / 5-(4-carboxy-phenyl)-10,15,20-tris-phenyl-porphyrin; k) tetrakis-(4-carboxy-phenyl)-porphyrin / $MnTa_2O_6$ (from manganese oxide); l) tetrakis-(4-carboxy-phenyl) porphyrin / $MnTa_2O_6$ (from manganese nitrate tetrahydrate); m) 5-(4-carboxy-phenyl)-10,15,20-tris-phenyl-porphyrin / $MnTa_2O_6$ (from manganese oxide); n) 5-(4-carboxy-phenyl)-10,15,20-tris-phenyl-porphyrin / $MnTa_2O_6$ (from manganese nitrate tetrahydrate) (*Contd*.)

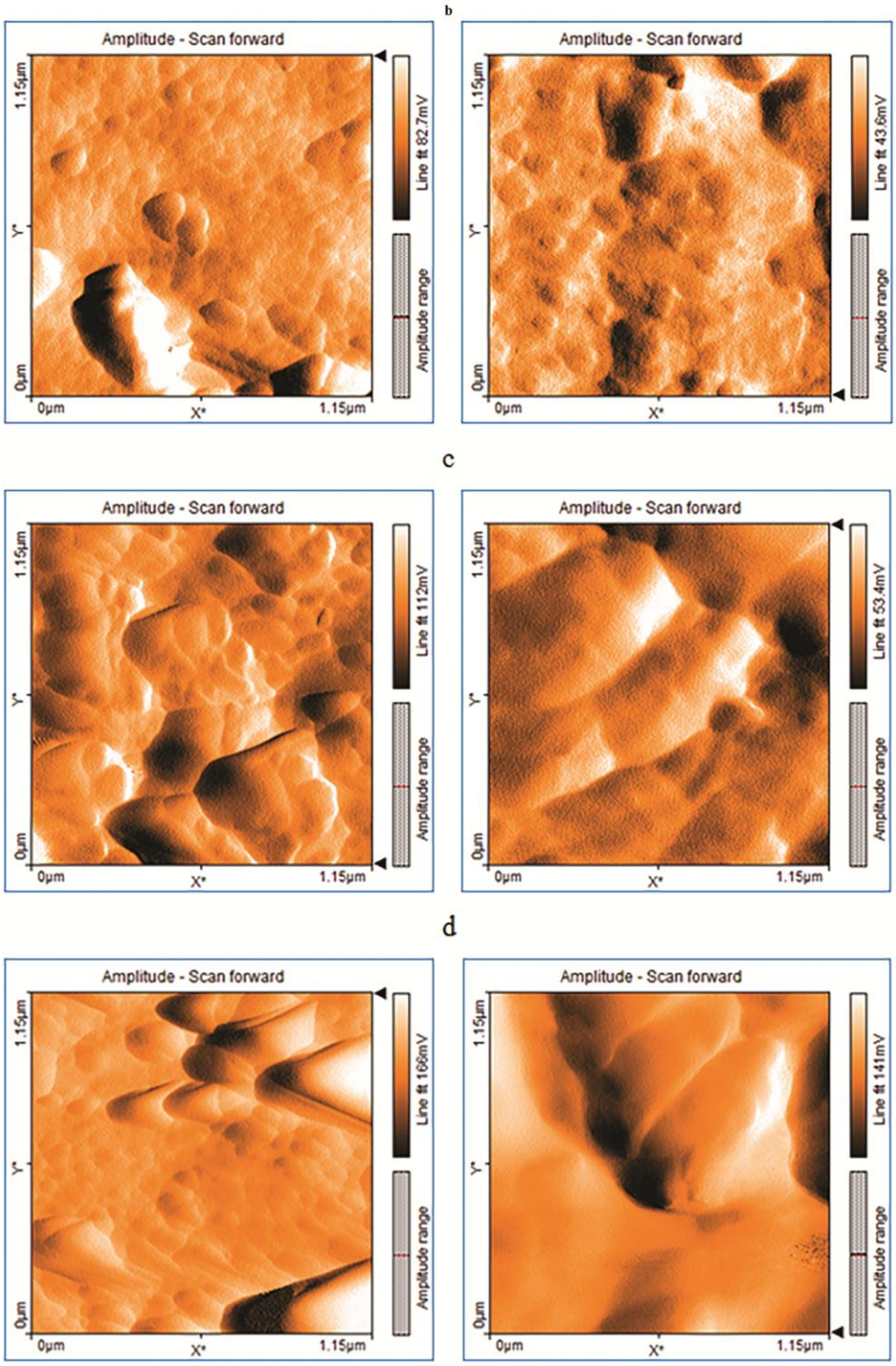

Fig. 4 — 2D AFM images for the depositions with the following structures before and after corrosion tests: OL (bare electrode), a) $MnTa_2O_6$ (from manganese oxide); b) $MnTa_2O_6$ (from manganese nitrate tetrahydrate); c) tetrakis-(4-carboxy-phenyl)-porphyrin; d) 5-(4-carboxy-phenyl)-10,15,20-tris-phenyl-porphyrin; e) $MnTa_2O_6$ (from manganese oxide) / tetrakis-(4-carboxy-phenyl)-porphyrin; f) $MnTa_2O_6$ (from manganese oxide) / 5-(4-carboxy-phenyl)-10,15,20-tris-phenyl-porphyrin; g) $MnTa_2O_6$ (from manganese nitrate tetrahydrate) / tetrakis-(4-carboxy-phenyl)-porphyrin; h) $MnTa_2O_6$ (from manganese nitrate tetrahydrate) / 5-(4-carboxy-phenyl)-10,15,20-tris-phenyl-porphyrin; k) tetrakis-(4-carboxy-phenyl)-porphyrin / $MnTa_2O_6$ (from manganese oxide); l) tetrakis-(4-carboxy-phenyl) porphyrin / $MnTa_2O_6$ (from manganese nitrate tetrahydrate); m) 5-(4-carboxy-phenyl)-10,15,20-tris-phenyl-porphyrin / $MnTa_2O_6$ (from manganese oxide); n) 5-(4-carboxy-phenyl)-10,15,20-tris-phenyl-porphyrin / $MnTa_2O_6$ (from manganese nitrate tetrahydrate) (*Contd*.)

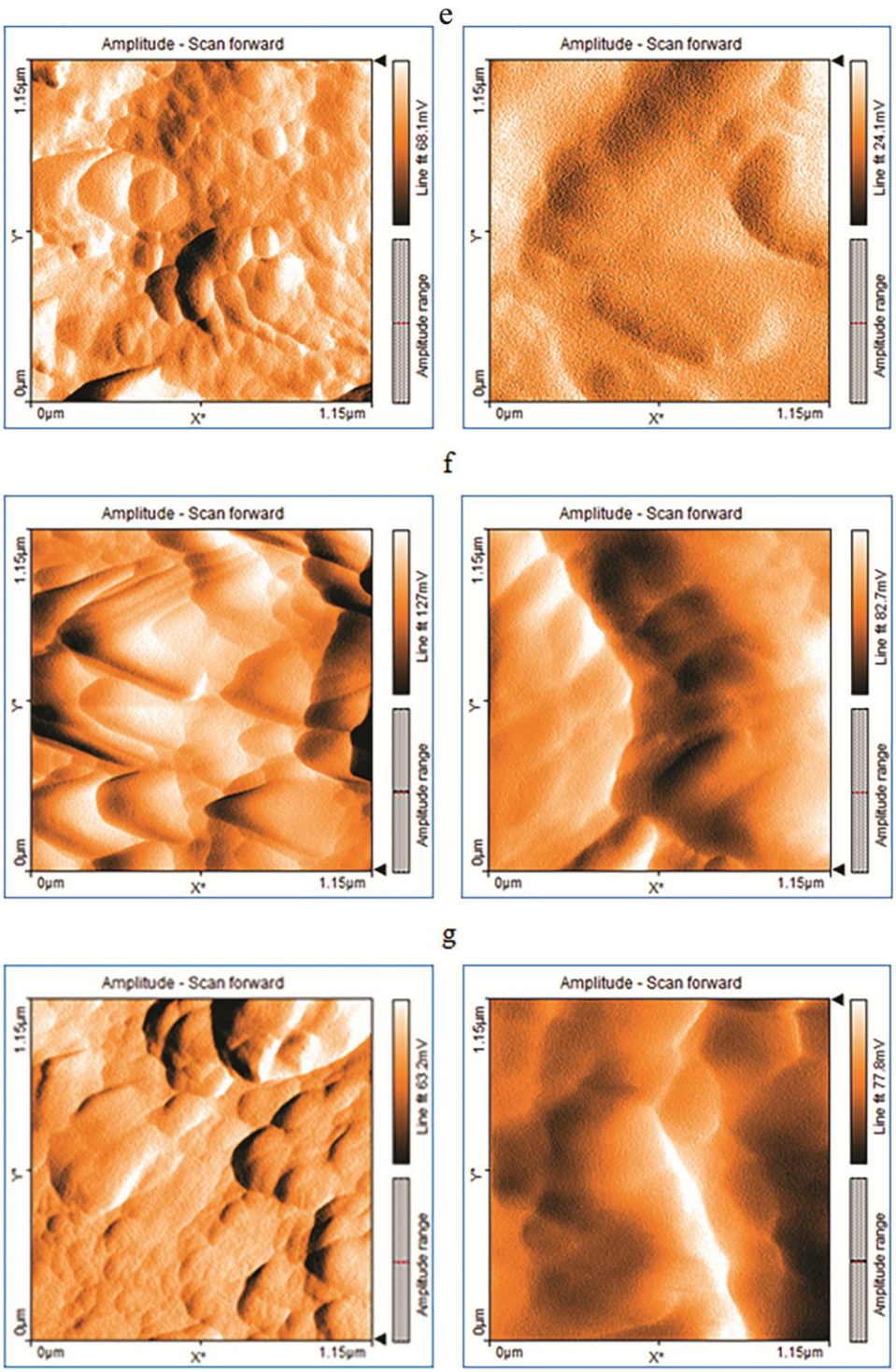

Fig. 4 — 2D AFM images for the depositions with the following structures before and after corrosion tests: OL (bare electrode), a) $MnTa_2O_6$ (from manganese oxide); b) $MnTa_2O_6$ (from manganese nitrate tetrahydrate); c) tetrakis-(4-carboxy-phenyl)-porphyrin; d) 5-(4-carboxy-phenyl)-10,15,20-tris-phenyl-porphyrin; e) $MnTa_2O_6$ (from manganese oxide) / tetrakis-(4-carboxy-phenyl)-porphyrin; f) $MnTa_2O_6$ (from manganese oxide) / 5-(4-carboxy-phenyl)-10,15,20-tris-phenyl-porphyrin; g) $MnTa_2O_6$ (from manganese nitrate tetrahydrate) / tetrakis-(4-carboxy-phenyl)-porphyrin; h) $MnTa_2O_6$ (from manganese nitrate tetrahydrate) / 5-(4-carboxy-phenyl)-10,15,20-tris-phenyl-porphyrin; k) tetrakis-(4-carboxy-phenyl)-porphyrin / $MnTa_2O_6$ (from manganese oxide); l) tetrakis-(4-carboxy-phenyl) porphyrin / $MnTa_2O_6$ (from manganese nitrate tetrahydrate); m) 5-(4-carboxy-phenyl)-10,15,20-tris-phenyl-porphyrin / $MnTa_2O_6$ (from manganese oxide); n) 5-(4-carboxy-phenyl)-10,15,20-tris-phenyl-porphyrin / $MnTa_2O_6$ (from manganese nitrate tetrahydrate) (*Contd*.)

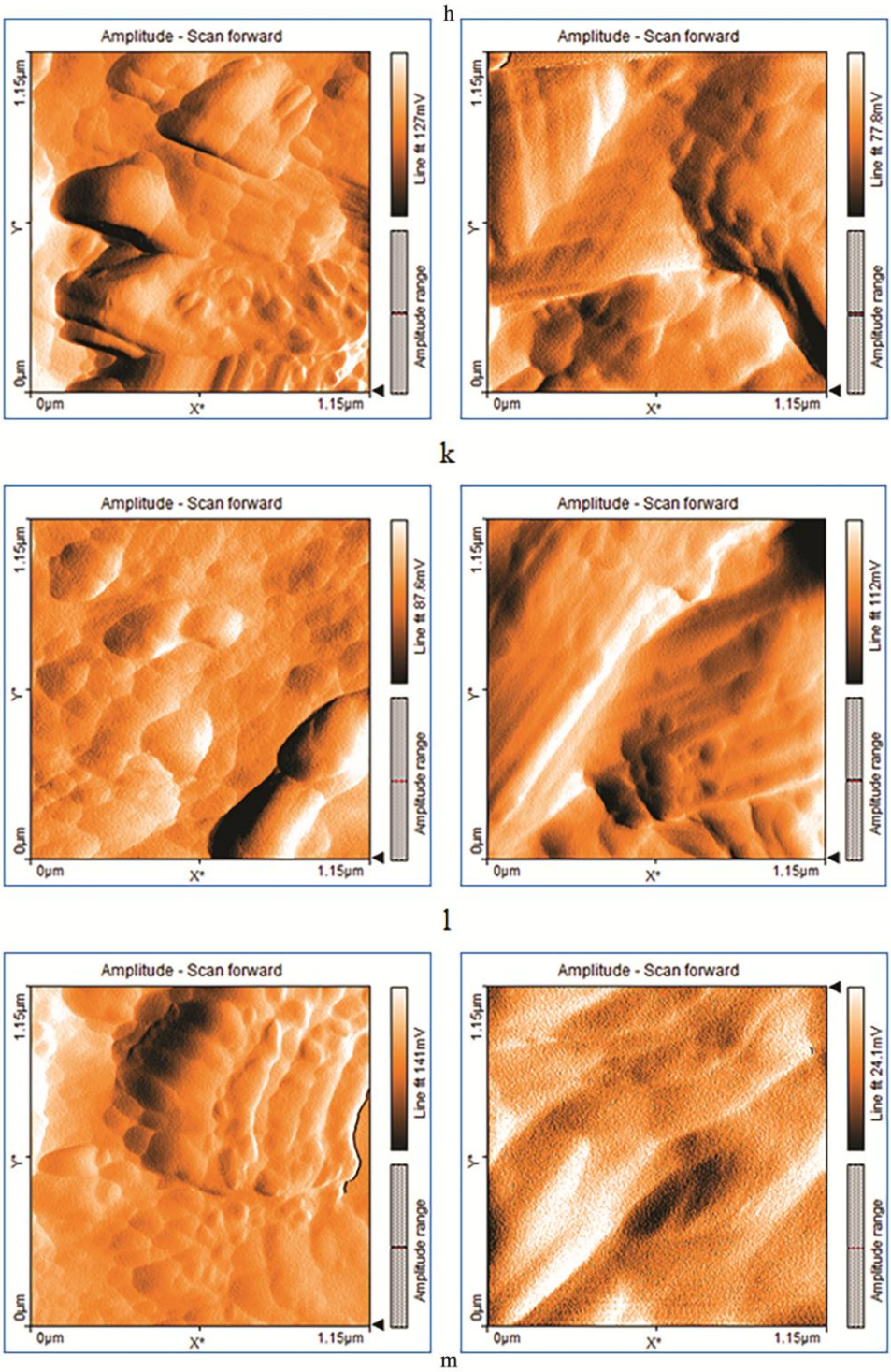

Fig. 4 — 2D AFM images for the depositions with the following structures before and after corrosion tests: OL (bare electrode), a) $MnTa_2O_6$ (from manganese oxide); b) $MnTa_2O_6$ (from manganese nitrate tetrahydrate); c) tetrakis-(4-carboxy-phenyl)-porphyrin; d) 5-(4-carboxy-phenyl)-10,15,20-tris-phenyl-porphyrin; e) $MnTa_2O_6$ (from manganese oxide) / tetrakis-(4-carboxy-phenyl)-porphyrin; f) $MnTa_2O_6$ (from manganese oxide) / 5-(4-carboxy-phenyl)-10,15,20-tris-phenyl-porphyrin; g) $MnTa_2O_6$ (from manganese nitrate tetrahydrate) / tetrakis-(4-carboxy-phenyl)-porphyrin; h) $MnTa_2O_6$ (from manganese nitrate tetrahydrate) / 5-(4-carboxy-phenyl)-10,15,20-tris-phenyl-porphyrin; k) tetrakis-(4-carboxy-phenyl)-porphyrin / $MnTa_2O_6$ (from manganese oxide); l) tetrakis-(4-carboxy-phenyl) porphyrin / $MnTa_2O_6$ (from manganese nitrate tetrahydrate); m) 5-(4-carboxy-phenyl)-10,15,20-tris-phenyl-porphyrin / $MnTa_2O_6$ (from manganese oxide); n) 5-(4-carboxy-phenyl)-10,15,20-tris-phenyl-porphyrin / $MnTa_2O_6$ (from manganese nitrate tetrahydrate) (*Contd*.)

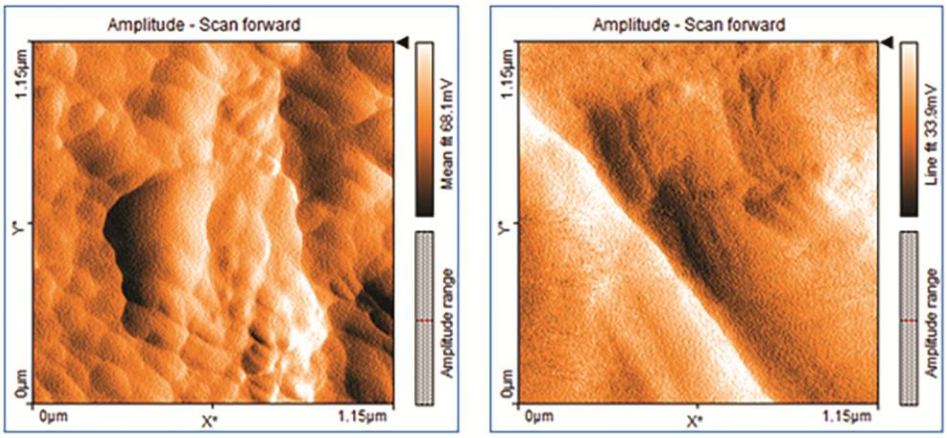

n

Fig. 4 — 2D AFM images for the depositions with the following structures before and after corrosion tests: OL (bare electrode), a) $MnTa_2O_6$ (from manganese oxide); b) $MnTa_2O_6$ (from manganese nitrate tetrahydrate); c) tetrakis-(4-carboxy-phenyl)-porphyrin; d) 5-(4-carboxy-phenyl)-10,15,20-tris-phenyl-porphyrin; e) $MnTa_2O_6$ (from manganese oxide) / tetrakis-(4-carboxy-phenyl)-porphyrin; f) $MnTa_2O_6$ (from manganese oxide) / 5-(4-carboxy-phenyl)-10,15,20-tris-phenyl-porphyrin; g) $MnTa_2O_6$ (from manganese nitrate tetrahydrate) / tetrakis-(4-carboxy-phenyl)-porphyrin; h) $MnTa_2O_6$ (from manganese nitrate tetrahydrate) / 5-(4-carboxy-phenyl)-10,15,20-tris-phenyl-porphyrin; k) tetrakis-(4-carboxy-phenyl)-porphyrin / $MnTa_2O_6$ (from manganese oxide); l) tetrakis-(4-carboxy-phenyl) porphyrin / $MnTa_2O_6$ (from manganese nitrate tetrahydrate); m) 5-(4-carboxy-phenyl)-10,15,20-tris-phenyl-porphyrin / $MnTa_2O_6$ (from manganese oxide); n) 5-(4-carboxy-phenyl)-10,15,20-tris-phenyl-porphyrin / $MnTa_2O_6$ (from manganese nitrate tetrahydrate)

Table 2 — Calculated surface roughness (the average roughness (S_a) and the mean square root roughness (S_q)) and the particle dimension on OL and covered electrodes

Electrode	Area(pm^2)	S_a (nm)	S_q (nm)	S_y (µm)	Particles dimension(nm)
OL		2.73	3.47	-	-
a		14.11	20.82	119.51	105
b		13.81	19.57	106.31	133
c		17.93	23.58	126.75	89.7
d		18.72	24.60	131.63	71.31
e	1.326	19.6	24.86	172.02	62
f		24.68	31.4	192.28	53.9
g		20.04	24.70	181.06	60
h		28.71	38.7	221.41	59
k		23.43	28.35	190.8	55.7
l		31.72	40.25	221.59	48.3
m		44.06	53.87	301.57	41.2
n		49.42	60.27	462.28	34

uniformity by adding the pseudo-binary oxide. On the other hand, the $MnTa_2O_6$ does not offer a sufficient protection alone and strongly needs the synergistic contribution of porphyrin.

The inhibition efficiencies (IE) were calculated based on equation (1) from[42] and for all the samples were obtained values of IE over 64% (Table 3).

$$IE\% = \left(1 - \frac{i_{corr}}{i^0_{corr}}\right) \times 100 \qquad \ldots(1)$$

Where i^0_{corr} and i_{corr} are the corrosion current densities in the absence and in the presence of the deposited protected layers on carbon steel electrodes.

As it can be seen in Table 3, where the calculated parameters from the Tafel plots are summarized, the corrosion current density (i_{corr}) of the OL electrode is 0.9548 mA/cm².

The highest inhibition efficiency of 95.48% was observed in the case of OL protected with 5-(4-carboxy-phenyl)-10,15,20-tris-phenyl-porphyrin /$MnTa_2O_6$ (obtained from manganese nitrate tetrahydrate) sandwich layers, that has a continuous shell-like morphology (Fig. 3n) and the value of corrosion current density more than 20 times lower than of not-protected OL, of only 0.0431 mA/cm². This deposition is also characterized by the highest value of thickness. As a general rule, there is a proportional relationship between the deposited layer thickness (Table 1) and the corrosion inhibition efficiency, which leads to the conclusion that the protection process is mechanical.

The polarization resistance (Rp) values of carbon steel material in 0.1M HCl increases from 101.35 $\Omega \cdot cm^2$ for bare OL to 143.91 $\Omega \cdot cm^2$ for 5-(4-carboxy-phenyl)-10,15,20-tris-phenyl-porphyrin / $MnTa_2O_6$ (from manganese oxide) (Table 3, m) indicating a significant inhibition of the corrosion process s when

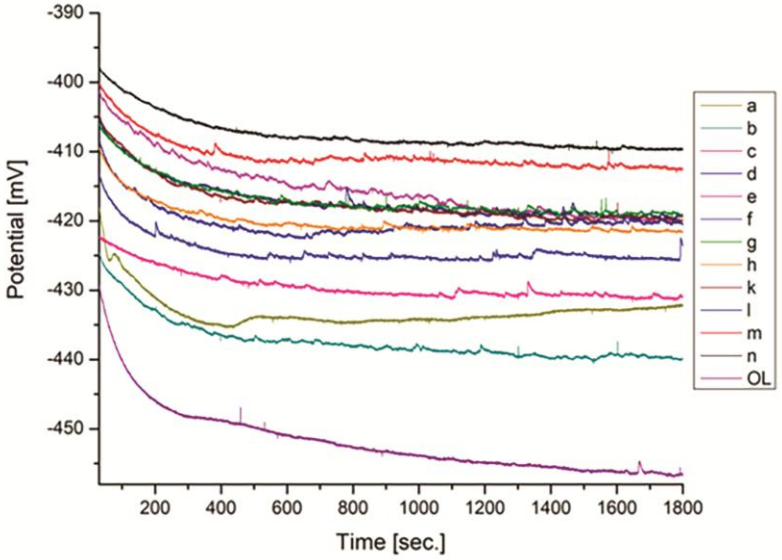

Fig. 5 — Evolution of open circuit potential with time for the investigated electrodes in 1 M HCl for: OL (bare electrode), a) $MnTa_2O_6$ (from manganese oxide); b) $MnTa_2O_6$ (from manganese nitrate tetrahydrate); c) tetrakis-(4-carboxy-phenyl)-porphyrin; d) 5-(4-carboxy-phenyl)-10,15,20-tris-phenyl-porphyrin; e) $MnTa_2O_6$ (from manganese oxide) / tetrakis-(4-carboxy-phenyl)-porphyrin; f) $MnTa_2O_6$ (from manganese oxide) / 5-(4-carboxy-phenyl)-10,15,20-tris-phenyl-porphyrin; g) $MnTa_2O_6$ (from manganese nitrate tetrahydrate) / tetrakis-(4-carboxy-phenyl)-porphyrin; h) $MnTa_2O_6$ (from manganese nitrate tetrahydrate) / 5-(4-carboxy-phenyl)-10,15,20-tris-phenyl-porphyrin; k) tetrakis-(4-carboxy-phenyl)-porphyrin / $MnTa_2O_6$ (from manganese oxide); l) tetrakis-(4-carboxy-phenyl)-porphyrin/ $MnTa_2O_6$ (from manganese nitrate tetrahydrate); m) 5-(4-carboxy-phenyl)-10,15,20-tris-phenyl-porphyrin / $MnTa_2O_6$ (from manganese oxide); n) 5-(4-carboxy-phenyl)-10,15,20-tris-phenyl-porphyrin / $MnTa_2O_6$ (from manganese nitrate tetrahydrate)

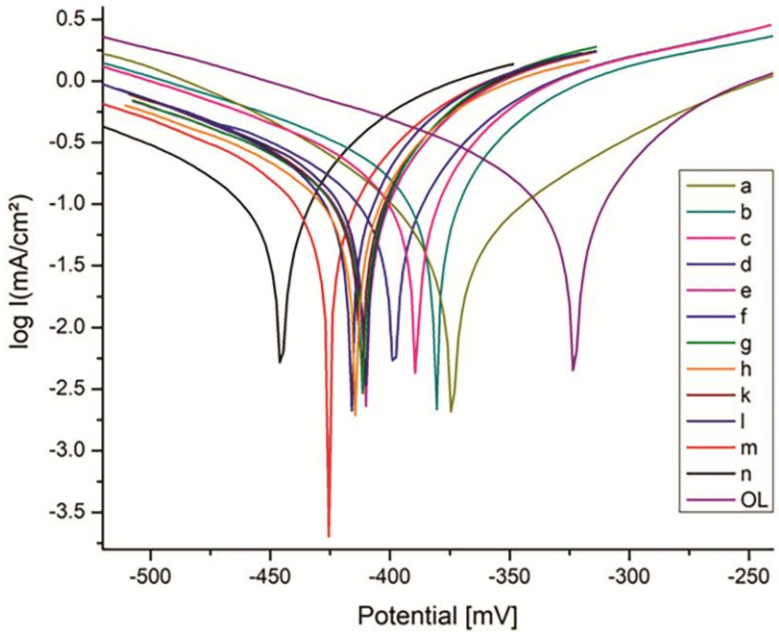

Fig. 6 — Tafel representation of polarization curves recorded in 1 M HCl for the investigated electrodes: OL (bare electrode), a) $MnTa_2O_6$ (from manganese oxide); b) $MnTa_2O_6$ (from manganese nitrate tetrahydrate); c) tetrakis-(4-carboxy-phenyl)-porphyrin; d) 5-(4-carboxy-phenyl)-10,15,20-tris-phenyl-porphyrin; e) $MnTa_2O_6$ (from manganese oxide) / tetrakis-(4-carboxy-phenyl)-porphyrin; f) $MnTa_2O_6$ (from manganese oxide) / 5-(4-carboxy-phenyl)-10,15,20-tris-phenyl-porphyrin; g) $MnTa_2O_6$ (from manganese nitrate tetrahydrate) / tetrakis-(4-carboxy-phenyl)-porphyrin; h) $MnTa_2O_6$ (from manganese nitrate tetrahydrate) / 5-(4-carboxy-phenyl)-10,15,20-tris-phenyl-porphyrin; k) tetrakis-(4-carboxy-phenyl)-porphyrin / $MnTa_2O_6$ (from manganese oxide); l) tetrakis-(4-carboxy-phenyl)-porphyrin/ $MnTa_2O_6$ (from manganese nitrate tetrahydrate); m) 5-(4-carboxy-phenyl)-10,15,20-tris-phenyl-porphyrin / $MnTa_2O_6$ (from manganese oxide); n) 5-(4-carboxy-phenyl)-10,15,20-tris-phenyl-porphyrin / $MnTa_2O_6$ (from manganese nitrate tetrahydrate)

Table 3 —Tafel parameters derived from potentiodynamic curves of carbon steel electrodes, unmodified and modified with mono- and bi-layers based on porphyrins and pseudo-binary oxides, after 30 minutes immersion in 0.1 M HCl.

Sample	Electrode	E_{corr} (mV)	Rp (Ωcm^2)	i_{corr} (mA/cm^2)	v_{cor} (mmY^{-1})	IE (%)
	OL	-406.3	101.35	0.9548	3.256	-
a	$MnTa_2O_6$ (from manganese oxide)	-419.6	120.74	0.3108	2.010	67.44
b	$MnTa_2O_6$ (from manganese nitrate tetrahydrate)	-416.9	105.87	0.3359	2.220	64.81
c	Tetrakis-(4-carboxy-phenyl)-porphyrin	-412.9	107.03	0.2879	1.893	76.23
d	5-(4-Carboxy-phenyl)-10,15,20-tris-phenyl-porphyrin	-417.2	136.33	0.1554	1.745	83.72
e	$MnTa_2O_6$ (from manganese oxide) / tetrakis-(4-carboxy-phenyl)-porphyrin	-410.3	116.70	0.1480	1.731	84.54
f	$MnTa_2O_6$ (from manganese oxide) / 5-(4-carboxy-phenyl)-10,15,20-tris-phenyl-porphyrin	-416.2	102.99	0.1396	1.853	85.39
g	$MnTa_2O_6$ (from manganese nitrate tetrahydrate) / tetrakis-(4-carboxy-phenyl)-porphyrin	-411.1	114.14	0.1476	1.726	84.54
h	$MnTa_2O_6$ (from manganese nitrate tetrahydrate) / 5-(4-carboxy-phenyl)-10,15,20-tris-phenyl-porphyrin	-414.3	125.21	0.1388	1.623	85.46
k	Tetrakis-(4-carboxy-phenyl)-porphyrin / $MnTa_2O_6$ (from manganese oxide)	-412.0	111.34	0.1446	1.678	84.85
l	Tetrakis-(4-carboxy-phenyl)-porphyrin / $MnTa_2O_6$ (from manganese nitrate tetrahydrate)	-410.0	103.90	0.1361	1.566	85.74
m	5-(4-Carboxy-phenyl)-10,15,20-tris-phenyl-porphyrin / $MnTa_2O_6$ (from manganese oxide)	-415.2	143.91	0.1362	1.546	86.72
n	5-(4-Carboxy-phenyl)-10,15,20-tris-phenyl-porphyrin / $MnTa_2O_6$ (from manganese nitrate tetrahydrate)	-417.7	128.64	0.0431	1.475	95.48

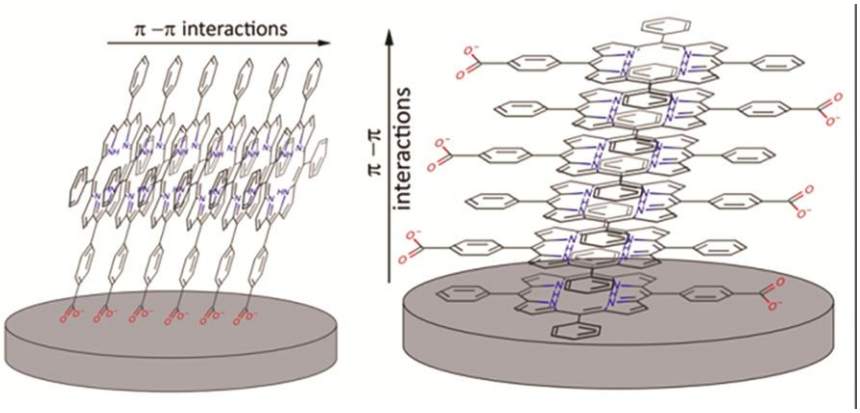

Fig. 7 — Mechanism of corrosion protection based on different types of porphyrin aggregation at the interface with steel surface

applying this type of sandwich structure onto its surface.

Taking into consideration the number of COOH functional groups grafted on porphyrin, it is clear that a better covering of the steel surface is realized if only one COOH anchor is used, characterized by better adherence (samples f, h, m, n), no matter of the deposition order. Even if comparing only the single layers deposited by the two porphyrins, there is a great difference of realized protection, namely, the 5-(4-carboxy-phenyl)-10,15,20-tris-phenyl-porphyrin (sample d) has an inhibition efficiency of 83.7%, significantly higher than that of 76.2% realized by tetrakis-(4-carboxy-phenyl)-porphyrin (sample c). We presume that the presence of four COOH groups modify the hydrophilic balance and might exfoliate from the surface of steel, or create a convex layer, allowing the aggressive media to enter into contact with the carbon steel.

The mechanism of protection might be due to more causes: a link based on affinity between the iron atoms and the porphyrin core, an anchoring on the electrode steel surface through COOH by OH bonds, and important π-π interactions between the units of porphyrins macrocycles, that are arranging on steel surface in compact vertical plane (because porphyrins are discotic molecules and form columnar self assembly) (Fig. 7).

On the other hand, the exposure of the porphyrin to the HCl induces aggregation and thus favours the protection against corrosion[44].

Conclusion

Drop-casting deposition of porphyrins and pseudo-binary oxides inorganic nanomaterials in the form of single and sandwich coatings is successfully performed on carbon steel disks, with the purpose of realizing corrosion inhibiting layers. All promoted materials act as corrosion inhibitors within a range from 67-95 % of inhibition efficiency for carbon steel.

There is a proportional relationship between the deposited layer thickness and the corrosion inhibition efficiency, which leads to the conclusion that the protection process is mechanically controlled.

The OL modified with deposited layers of 5-(4-carboxy-phenyl)-10,15,20-tris-phenyl-porphyrin / $MnTa_2O_6$ (derived from manganese nitrate tetrahydrate) show the best corrosion resistance (over 95%) in comparison with the other types of depositions.

In conclusion, a better covering of the steel surface is realized if only one COOH anchor is used, characterized by better adherence. It is presumed that the presence of four COOH groups modify the hydrophilic balance and might exfoliate from the surface of steel, or create a convex layer, allowing the aggressive media to enter into contact with the carbon steel.

Acknowledgements

This work was supported by grant of the Romanian Ministry of Research, Innovation and Digitization/UEFISCDI, project number PN-III-P2-2.1-PED-2019-0487, 528PED/2020, CeraPor-Corrand partially by Romanian Academy through Programme 3/2022 from Institute of Chemistry "Coriolan Dragulescu".

References

1 Malik M A, Hashim M A, Nabi F, AL-Thabaiti S A & Khan Z, *Int J Electrochem Sci*, 6 (2011) 1927.
2 Liu Y, Liang X, Gu L, Zhang Y, Li G D, Zou X & Chen J S, *Nat Commun*, 9 (2018) 2609.
3 Yang H, Gong L, Wang H, Dong C, Wang J, Qi K, Liu H, Guo X & Xia B Y, *Nat Commun*, 11 (2020) 5075.
4 Wang M, Dong C L, Huang Y C & Shen S, *ACS Catal*, 10 (2020) 1855.
5 Vijayalakshmi K, Punitha N, Rengamy R & Elangovan J, *Indian J Chem Technol*, 28 (2021) 421.
6 Zou X, Wu Y, Liu Y, Liu D, Li W, Gu L, Liu H, Wang P, Sun L & Zhang Y, *Chem*, 4 (2018) 1139.
7 El-Haddad M A M, Bahgat Radwan A, Sliem M H, Hassan W M I & Abdull A M, *Sci Rep*, 9 (2019) 3695.
8 Jayakumar S P, Murugadoss V & Angaiah S, *Indian J Chem Technol*,28 (2021) 385.
9 Aghili M, Yazdi M K,Ranjbar Z & Jafari S H, *Corros Sci*, 179 (2021) 109143.
10 Birdeanu M, Vaida M & Fagadar-Cosma E, *Manuf Rev*, 7 (2020) 1.
11 Zinad D S, Jawad Q A, Hussain M A M, Mahal A, Mohamed L & Al-Amiery A A, *Int J Corros Scale Inhib*, 9 (2020) 134.
12 Birdeanu M, Epuran C, Fratilescu I & Fagadar-Cosma E, *Processes*, 9 (2021) 1890.
13 Goyal M, Vashisht H, KumarA, Kumar S, Bahadur I, Benhiba F & Zarrouk A, *J Mol Liq*, 316 (2020) 113838.
14 Laabaissi T, Benhiba F, Rouifi Z, Missioui M, Ourrak K, Oudda H, Ramli Y, Warad I, Allali M & Zarrouk A, *Int J Corros Scale Inhib*, 8 (2019) 241.
15 Kerkour R, Chafaa S, Maouche N, Moumeni O & Chafai N, *Indian J Chem Technol*, 26 (2019) 69.
16 Birdeanu M, Bîrdeanu A V, Vaida M, Milovanovic D, Lascu A & Fagadar-Cosma E, *Phys Sci*, 94 (2019) 075702.
17 BîrdeanuA V, Birdeanu M & Fagadar-Cosma E, *J Alloys Compds*, 706 (2017) 220.
18 Vaida M, Birdeanu M & Bîrdeanu A V, *AIP Conf Proc*, 2071 (2019) 040017.
19 Bîrdeanu A V, Vaida M, Milovanovic D, Petronic S & Birdeanu M, *Adv Mat Res*, 4 (2018) 149.
20 Birdeanu M, Birdeanu A V, Vaida M, Orha C & Fagadar-Cosma E, Anticorrosive properties of $ZnTa_2O_6$ and ZnV_2O_6 nanomaterials deposited as sandwich structures by drop casting method inNaCl, *Conference Proceedings 9th International Conference on Nanomaterials - Research & Application*, (Brno, Czech Republic), 2018.
21 Hu W, Xu J, Lu X, Hu D, Tao H, Munroe P &Xie Z H, *Appl Surf Sci*, 368 (2016)177.
22 BelineT, de Almeida A B, Neto N F A, Matos A O, Ricomini-Filho A P, Sukotjo C, Smeets P J M, da Silva J H D, NocitiJr F H & Barao V A R, *Appl Surf Sci*, 520 (2020) 146326.
23 Ding Z, Zhou Q, Wang Y, Ding Z, Tang Y & He Q, *Ceram Int*, 47 (2021) 1133.
24 Zhang S, Tian Y, Guo Y, Shan J & Liu R, *Chemosphere*, 262 (2021) 127904.
25 Nurislamova E A, Ziganshina M R, Stepin S N & Mendelson V A, *Mater SciEng*, 905 (2020) 012051.
26 Cao Z F, Wang J, Qiu P, Yang F, Wang S, Liu G & Zhong H, *Surf Coat Technol*, 347 (2018) 235.
27 Lu F, Cao Z F, Yang F, Wang S & Zhong H, *Prog Org Coat*, 132 (2019) 379.
28 Gulyaeva R I, Petrova S A, Chumarev V M & Selivanov E N, *J Alloys Compds*, 834 (2020) 155153.
29 Mehmeti V & Podvorica F I, *Materials*, 11 (2018) 893.
30 Ding Z, He Q, Ding Z, Liao C, Chen D & Ou L, *Nanomaterials*, 9 (2019) 685.
31 Hou J, WangY, Yuan Z, Cai H & Chen W, *Int J Electrochem Sci*, 16 (2021) 210764.
32 Bordbar-Khiabani A, Bahrampour S, Mozafari M & Gasik M, *Ceram Int*,48 (2022) 3148.
33 Wei D B, Chen X H, Zhang P Z, Ding F, Li F K &Yao Z J, *Appl Surf Sci*, 441 (2018) 448.
34 Yao J, Cheng Y, Zhou M, Zhao S, Lin S, Wang X, Wu J, Li S &We H, *Chem Sci*, 9 (2018) 2927.
35 Manso A P, Marzo F F, Garicano X, Alegre C, Lozano A & Barreras F, *Int J Hydrogen Energy*, 45 (2020) 20679.
36 Nikrooz B, Ebrahimifar H & Zandrahimi M, *Indian J Chem Technol*, 24 (2017) 162.

37 Sebarchievici I, Tăranu B O, Birdeanu M, Rus S F & Fagadar-Cosma E, *Appl Surf Sci*, 390 (2016) 131.

38 Taranu B, Sebarchievici I, TaranuI, Birdeanu M & Fagadar-Cosma E, *Rev Chim*, 67 (2016) 892.

39 Birdeanu M, Vaida M, Bîrdeanu A V & Fagadar-Cosma E, *Corros*, 76 (2020) 734.

40 Fagadar-Cosma E, Vlascici D, Birdeanu M & Fagadar-Cosma G, *Arab J Chem*, 12 (2019) 1587.

41 Wagner R W, Lawrence D S & Lindsey J S, *Tetrahedron Lett*, 28 (1987) 3069.

42 Ahmad Z, *Principles of Corrosion Engineering and Corrosion Control*, (Butterworth-Heinemann, Oxford, UK), 2006, 377.

43 Kapaklis V, Poulopoulos P, Karoutsos V, Manouras T & Politis C, *Thin Solid Films*, 510 (2006) 138.

44 Krieger A, Werner J P F, Mariani G &Gröhn F, *Macromolecules*, 50 (2017) 3464.